Journal of Physics: Conference Series

PAPER • **OPEN ACCESS**

Difference of co-extracted electron current and beam acceleration in a negative ion source with hydrogen-isotope ions

To cite this article: K. Ikeda *et al* 2022 *J. Phys.: Conf. Ser.* **2244** 012060

Difference of co-extracted electron current and beam acceleration in a negative ion source with hydrogen-isotope ions

K. Ikeda[1], K. Tsumori[1,2] H. Nakano[1,3], K. Nagaoka[1,3], Y. Takeiri[1], S. Masaki[2] , E. Rattanawongnara[2] and M. Osakabe[1,2]

[1] National Institute for Fusion Science (NIFS), National Institutes of Natural Sciences, Toki, 509-5292, Japan
[2] The Graduate University for Advanced Studies, SOKENDAI, Toki 509-5292, Japan
[3] Graduate School of Science, Nagoya University, Nagoya 464-8603, Japan

E-mail: ikeda.katsunori@nifs.ac.jp

Abstract.
Improvement of the performance on a hydrogen/deuterium negative ion source for a nuclear fusion device is reported. In particular, the suppression of the co-extracted electron current, I_e, is an important issue to ensure the stable beam acceleration. Improvement of the I_e has been confirmed by optimizing the magnetic field of the electron deflection magnet in the extraction grid. Two other new methods for reduction of the I_e were validated. The first was an electron fence whose rods were set between the rows of apertures on a plasma grid. The electron and negative ion current ratio, approximately I_e/I_{acc}, was greatly improved from 0.7 to 0.25 in deuterium. The second was an outer iron yoke which enhanced the magnetic flux density 19% inside the arc discharge chamber. The I_e/I_{acc} using the outer yoke decreased by 0.1 compared with using a normal magnetic filter in a deuterium operation. These attempts have improved the total deuterium injection beam power of 8.4 MW by three negative ion based NBIs.

1. Introduction

High-energy and high-current neutral beam injection (NBI), using negative ion sources called N-NBI, is an important tool for efficient plasma heating and current drive, and for delivering fuel particles in the field of plasma-based fusion. These fusion devices require hydrogen isotopes such as deuterium (D) and tritium (T). N-NBI systems have been practically applied in the large helical device (LHD) [1–5], the JT-60U [6, 7] and the JT-60SA [8] where stable high-energy deuterium beams have been used for plasma experiments. The ITER tokamak, which is under construction in France [9], will use N-NBI to produce 1 MeV deuterium negative ion beams [10–12]. Tritium and deuterium as a fuel are essential for fusion plants, however the exsisting amount of tritium is limited on the earth [13]. On the other hand, tritium is produced by DD fusion reactions in the reactor, therefore it is desirable to reuse DT molecules in the evacuation gas, as a mixed isotope beam source [14]. For these reasons, the efficiency of negative ion production of hydrogen isotopes, the difference of isotope beam acceleration, and the suppression of co-extracted electron current are important issues in negative ion source engineering.

Three N-NBIs called BL1, BL2 and BL3 for plasma production and heating are operated in the LHD; their negative ion sources are optimized for hydrogen (H) [2]. Both hydrogen and deuterium beam injection have been carried out for deuterium experiments in the LHD [15, 16]. It is possible to compare production of negative ions and their beam characteristics between hydrogen isotopes using a hydrogen optimized negative ion source. Therefore, the following four points of the isotope beam are interesting subjects. (i) Production of isotope negative ions and the extraction property of the negative ion current. (ii) Differences in stripping loss in the accelerator. These topics have a direct effect on the output beam power. (iii) Optical property of the isotope beam, which affects the heat load on the injector equipment and the port through efficiency. (iv) Co-extracted electron current [I_e], which is unique to negative ion sources and is very important in terms of preventing damage to the grid system by electrons.

This paper presents the history of the maximum neutral beam injection power of H and D beams on the NBIs in the LHD. Injection beam power in deuterium negative ions produced by a hydrogen optimized negative ion source decreased due to decreasing the negative ion current, increasing the stripping loss rate, and expansion of the beam width. The high power arc discharge required for high power beam generation is limited by the increase in the I_e. Two methods of effectively reducing the I_e will be reported.

2. Performance of hydrogen isotope beam injection

2.1. Injected beam power

The nominal acceleration drain current [I_{acc}] of hydrogen negative ions and the beam energy [E_{beam}] for the N-NBI in the LHD are 80 A and 180 keV, respectively, by two arc discharge type negative ion sources. The extracted beam power of negative ions is 14.4 MW, however the nominal beam injection power is 5 MW because the port through efficiency including neutralization and re-ionization is approximately 0.35. The standard beam pulse width is 2 seconds. Deuterium beam operation was initiated in 2017 using hydrogen optimized negative ion sources by switching the operation gas between H_2 and D_2. The hydrogen beam was used as an important heating source in high ion temperature plasma experiments, and the deuterium beam was used as a driver for neutron production in DD fusion experiments.

Figure 1 shows the history of the maximum port through power of both H (opened marks) and D (closed marks). The circle, square, and triangle marks indicate the values of BL1, BL2, and BL3, respectively. Maximum deuterium beam power improved from 7 MW to 8.4 MW in the latest experimental campaign. The negative ion source of TOSHIBA-type at BL1 uses a hexagonal arc chamber, which has good arc power efficiency on the hydrogen negative ion current [17]. The beam power of 6.2 MW in hydrogen was injected. However, the deuterium beam power was significantly reduced because of the increase in the I_e, which is defined by subtracting the I_{acc} from the extraction current [I_{ext}]. An electron fence performed well to suppress the I_e, and the injection beam power improved 3 MW in 2020. BL2 and BL3 are equipped with HITACHI-type ion source which uses a rectangle cross section arc chamber [2]. The two types of ion sources produce beams of the same size. The injection power of the hydrogen beam at BL2 reduced to 3.4MW, due to the decrease in the port through efficiency below 0.3 after the deuterium operation. The deuterium beam injection power was 2.4 MW in the latest campaign. On the other hand, the tangential injection direction of BL2 is opposite to the direction of BL1 and BL3. Therefore a stable supply of high power hydrogen beam is required on the BL2 for toroidal current control in the LHD. The BL2 will be operated on a conventional multi-aperture grounded grid [18] to focus on hydrogen beam operation in the next experimental campaign in 2021. The BL3 injected 4.4 MW hydrogen beam which slightly decreased before the deuterium operation, and the port through efficiency was maintained at 0.35. Deuterium beam injection of 3 MW has been achieved by modifying the accelerator gap setting [4]. Since this injector worked as a benchmark to verify suppression of the I_e on the

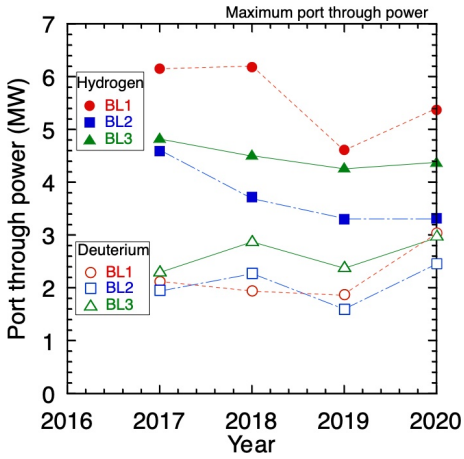

Figure 1. History of maximum port through power from N-NBI in LHD. Circle, square, and triangle marks indicate values of BL1, BL2, and BL3, respectively. Closed and opened marks are cases of hydrogen and deuterium beams, respectively.

deuterium beam operation, the effects of a bias voltage and a filter field strength on the I_e were also investigated.

2.2. Issues of deuterium beam acceleration

The negative-ion current linearly increased with respect to the arc discharge power and was not saturated. The averaged ratio of the deuterium current to the hydrogen current $[I_{acc(D)}/I_{acc(H)}]$ was approximately 0.66 for the same arc discharge power [4]. The reduction ratio in the injection beam power was below the reduction ratio in the negative ion current. Therefore, the discussion of the port through efficiency is important for the moderate beam injection power in deuterium. Figure 2 shows the shot history of the horizontal full width at half maximum (FWHM) of the negative ion beam, measured by the beam calorimeter, at the 8 m downstream from the ion source. The beam width in the horizontal direction consists of 14 beamlets, and in the vertical direction there are 55 beam rows. The FWHM of the hydrogen beam is 160 mm, however that of the deuterium beam expands to over 190 mm by switching operation gas. The divergence of the charged particle beamlet is caused by the self potential generated space-charge, perpendicular to the beam direction. Deuterium beams with larger mass numbers have larger divergence angles compared with hydrogen beams. Furthermore, the negative ion beam is bent by the magnetic field of an electron deflection magnet (EDM) installed in the extraction grids (EG) to prevent co-extracted electrons entering into the acceleration region. Deflection of the negative ion beams in hydrogen is corrected using the axial displacement of the steering grid apertures. However, this axial displacement is not corrected with the deuterium beam. For this reason, the deuterium beam width is expanded by shifting the beam direction alternately for each beamlet row group.

Another reason for reduction of the injection beam power is the stripping loss. Figure 3(a) shows the beam emission spectra both H (dashed line) and D (bold lime) observed at the 1 m downstream of the ion source. The optical line of sight is set 33° to the center of beam line. The E_{beam} is 171 keV including the extraction voltage of 9 kV in both cases. All peaked spectral lines are Balmer-alpha lines for hydrogen (H_α) and deuterium (D_α). The most intense line is the background light from the ion source, and the light from the full-energy beam appears at 646 nm and 649 nm for H and D, respectively, due to the Doppler effect. No clear peaks appear in the high-energy region near the full-energy peak; however asymmetric peaks are observed in the low-energy region near the background spectra. Figure 3(b) shows the beam emission

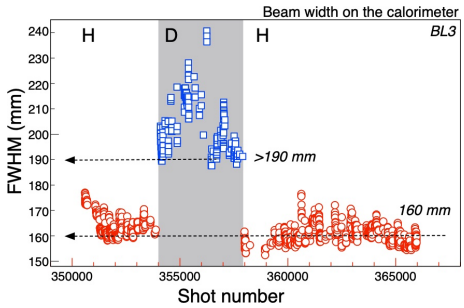

Figure 2. History of beam width (FWHM) on beam calorimeter for hydrogen (circle marks) and deuterium (square marks) beam operation.

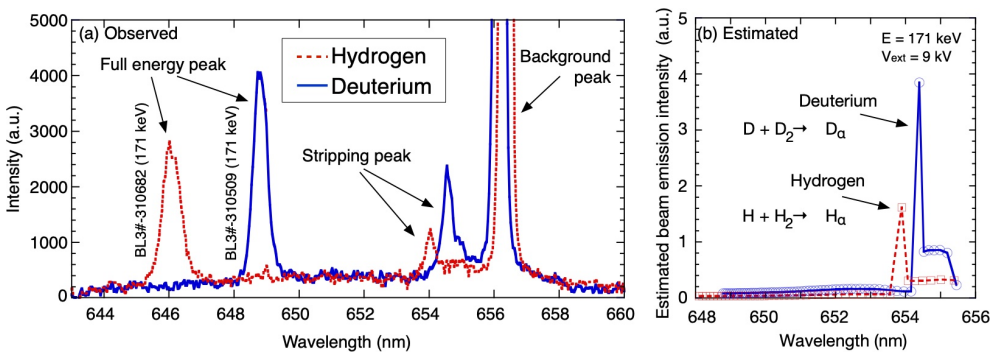

Figure 3. (a)Observed beam emission spectra for hydrogen (dashed line) and deuterium (bold line). (b) Estimated beam emission spectra by distributions of vacuum pressure and stripping loss neutrals in beam accelerator. Reproduced from [19], with permission of AIP Publishing.

spectrum estimated by calculating the number of neutralized particles from the vacuum pressure and energy distributions inside the accelerator from the plasma grid (PG) to the grounded grid (GG). The low-energy stripping peak corresponds to the energy of the extraction voltage (9 keV). This is a beam particle neutralized in the EG apertures by the high neutralization efficiency, due to 83% of the ion source pressure and low energy, and is a major component of stripping loss. In particular, the EG has a thickness of 14 mm due to the EDM and water cooling channels, which is a disadvantage in stripping loss. The neutralization reaction between the PG and EG also produces very low energy neutrals, therefore the stripping peak forms an asymmetric shape with a large tail on the low energy side. The stripping peak does not appear in the high energy acceleration region, which is consistent with the observed results. The amount of stripping loss in the accelerator is 16% and 24% for hydrogen and deuterium, respectively. Therefore, the stripping loss during beam acceleration of heavy isotopes is larger than that of light isotopes.

3. Improvement of the co-extracted electron current

The ratio of co-extracted electron current and the negative ion current is an important indicator for the safe operation of a negative ion source. Even in a large RF-discharge type negative ion source for ITER-NBI, which is currently under development, the electron current and ion ratio is required to be less than 1 for the deuterium operation. The low electron and ion current ratio of $0.2 < I_e/I_{acc(H)} < 0.25$ was achieved on hydrogen operation using the arc-discharge type negative ion source in LHD-NBI. On the other hand, the $I_e/I_{acc(D)}$ increased more than

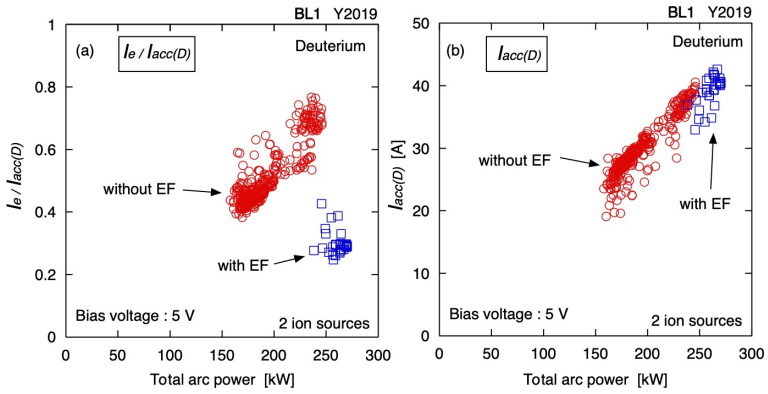

Figure 4. (a)Averaged $I_e/I_{acc(D)}$ using two ion sources in deuterium operation. Circle and square marks show original PG without EF and with EF, respectively. (b) Total $I_{acc(D)}$ using two ion sources in deuterium operation.

0.35 on deuterium operation, which is the critical issue for high power beam injection using high arc-discharge power. Increasing the bias voltage applied to the PG and changing the extraction gap length were effective in reducing the $I_e/I_{acc(D)}$ [5]. Recently, two other methods were found to reduce $I_e/I_{acc(D)}$ effectively.

3.1. Electron fence

An egg-box cell structure on the PG surface was tested in the small negative ion source at NIFS in the 1990s [20]. The egg-box cell was effective in reducing the electron current, however it did not increase the hydrogen negative ion current. The egg-box cell was a complex structure combination of 2 mm thin molybdenum plates. Therefore, thermal deformation was difficult to control in high-current ion sources for injectors that require high arc power discharge. An electron fence (EF) was developed to apply the electron suppression effect of the egg-box cell to deuterium discharges, and was installed into the negative ion source of BL1 [21]. The EF has a simple and robust structure made of 5 mm diameter molybdenum rods, which was placed between the rows of apertures on the PG surface in parallel to the EDM installed in the EG. The top of the EF was initially set at 5 mm from the PG, then this position was changed at 7 mm in 2020, which is as same height as the egg-box cell. The electrical potential of the EF was the same as the PG, and a positive bias voltage was also applied to the EF. The magnetic field lines produced by the EDM exit between the rows of PG apertures, pass through the EF, and cross the over the PG apertures; the EF is expected to absorb magnetized electrons trapped in the magnetic field lines produced by the EDM. Figure 4(a) and 4(b) are the averaged $I_e/I_{acc(D)}$ and the total $I_{acc(D)}$, respectively, in deuterium discharge with Cs vapor from two ion sources. In the case without an EF (circle marks), the $I_e/I_{acc(D)}$ exceeded 0.7 for a total arc discharge of 250 kW. This increase in the I_e limited the use of high arc power discharges. The TOSHIBA-type negative ion source for BL1 had good arc power efficiency of H^- ion current, however a large increase in electron current was observed compared with the HITACHI-type source in the deuterium operation. However, the $I_e/I_{acc(D)}$ decreased to 0.25 using the EF (square marks), which was low enough to operate the negative ion source in deuterium, as in the case of hydrogen discharge. The reduction of I_e enabled a high current negative ion beam by high arc power discharge, however the arc power efficiency was not changed. These properties of the EF were consistent with the egg-box cell.

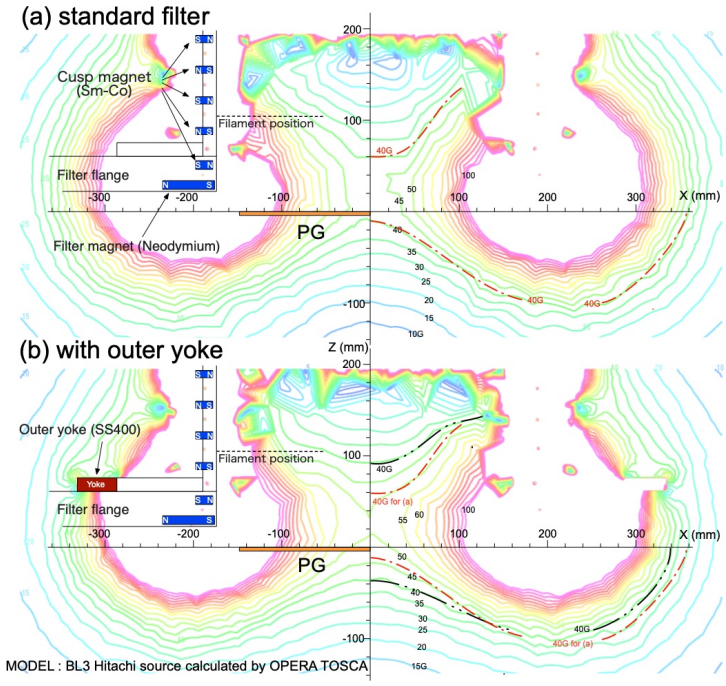

Figure 5. Distribution of magnetic flux density calculated by OPERA simulation software [24] using full magnetic model for arc discharge chamber of HITACHI-type source in BL3. (a) and (b) show cases of standard filter and extended filter using outer iron yoke, respectively. Left half of figure from center shows position of magnets and outer yoke. Magnets in right half are set symmetrical to center axis and its polarity is reversed.

3.2. Outer iron yoke

An external magnetic filter had been reported to be effective in enhancing the negative ion current and suppressing the I_e in an arc discharge type negative ion source [22, 23]. In the negative ion source for LHD-NBI, an insulating plate and a magnetic filter flange were inserted between the PG and the arc chamber to suppress the inflow of charged particles in the vicinity of the PG. Effects of the external magnetic filter were verified only for hydrogen discharge, therefore verification is needed whether the standard magnetic filter is matched for deuterium discharges. However, it is difficult to verify the filter effect by replacing the permanent magnets, because these magnets are installed inside the vacuum boundary of the magnetic filter flange. Therefore, an iron yoke is installed outside the vacuum vessel to increase the filter magnetic field strength inside the arc chamber. Fig. 5(a) shows a cross-sectional view of the arrangement of the magnets of the BL3 negative ion source in the short direction. The left half of figure from the center shows the position of the magnets. Samarium-cobalt magnets that create a cusp magnetic field are placed on the side wall and back plate. The external filter magnet is a neodymium magnet located at z = 30 mm from the PG surface. Both magnets in the right half are set symmetrical to the center axis and the polarity is reversed. Figure 5(a) also shows the contour plot of magnetic flux density [B] created by the cusp magnets and filter magnets, which is calculated by the OPERA simulation software [24]. The maximum B on the z-axis is 42 G, which corresponds to the position of the filter magnet at z = 30 mm. The magnetic field strength on the center axis, i.e. x = 0 mm, is the minimum value. The region above 40 G (single-dotted line) distributes to z = 60 mm in the standard filter case. Figure 5(b) shows the B distribution using the outer iron yoke. The yoke is made of structural steel (Japanese Industrial

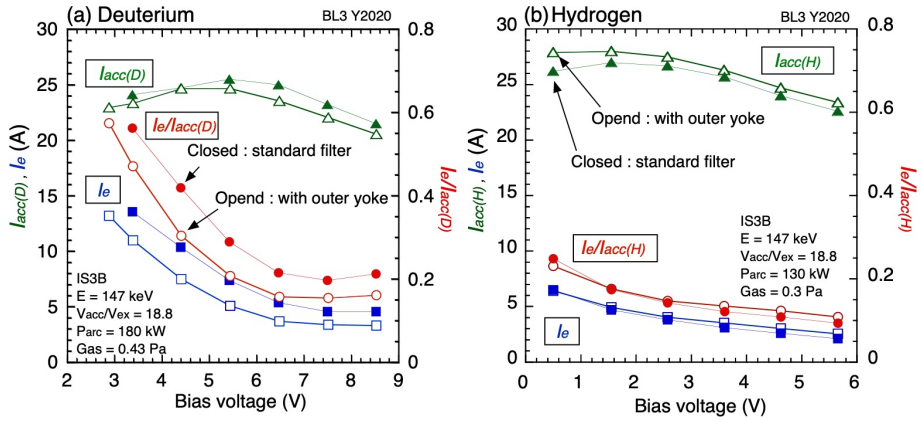

Figure 6. (a) Dependence of $I_{acc(D)}$ (triangle), I_e (square), and $I_e/I_{acc(D)}$ (circle) on bias voltage. (b) Dependence of $I_{acc(H)}$ (triangle), I_e (square), and $I_e/I_{acc(H)}$ (circle) on bias voltage. Closed marks and opened marks show cases of standard filter and extended filter, using outer iron yoke, respectively.

Standard SS400) with a cross-sectional size of 50 mm wide and 16 mm thickness. The side wall of the arc chamber has the terminal of the filament, which restricts the installation space for the outer yoke. Therefore, the outer yoke is placed on the filter flange around the four sides of the arc chamber flange. The outer yoke reduces the outer magnetic field strength and increases the magnetic field strength inside the vacuum vessel. The maximum B on the z-axis is 50 G, which corresponds to the position of the filter magnet at z = 30 mm. The outer yoke affects not only the filter magnet but also the cusp magnet, and the region above 40 G (double-dotted line) is extended to z = 90 mm. The weak magnetic field region, i.e. the confining plasma region, is considered to be shifted toward the back plate. This extended filter arrangement is expected to suppress the inflow of charged particles into the vicinity of the PG surface.

The effect of the outer iron yoke on hydrogen and deuterium discharges using a HITACHI-type negative ion source in BL3. Figures 6 show the bias voltage dependence of the negative ion and electron currents in the deuterium and hydrogen operation. Triangles, squares, and circles are I_{acc}, I_e, and I_e/I_{acc}, respectively. The closed and open marks are the standard filter and enhanced filter with outer iron yoke, respectively. Only one ion source was operated in this experiment which was different from the normal injector operation. The order of the NBI operation gas and filter condition was H_2 with the standard filter, D_2 with the standard filter, D_2 with the enhanced filter, and H_2 with the enhanced filter. In the deuterium discharge, a decrease in the I_e was clearly observed by the enhanced filter with the outer iron yoke in the entire bias voltage range, as shown in Fig. 6(a). The bias voltage of 5.6 V was applied in the normal deuterium operation with the standard filter, which produced the highest deuterium negative ion current and a reasonably low electron current. In low bias voltage operation, the operating region was limited by a large increase in electron current. However, a low bias voltage of 4.2 V provided good beam performance with low $I_e/I_{acc(D)} = 0.3$ using an enhanced magnetic filter by an outer iron yoke. At a bias voltage of 5.6 V, $I_e/I_{acc(D)}$ was 0.2 which was equally low as the $I_e/I_{acc(H)}$ in a high-arc power discharge in the hydrogen operation.

On the other hand, in the hydrogen discharge shown in Fig. 6(b), the I_e and the $I_e/I_{acc(H)}$ did not change when the filter field was enhanced by installing the outer iron yoke. The $I_{acc(H)}$ increased slightly on the enhanced filter. This result suggests that the use of an enhanced filter for deuterium does not have a negative effect on the hydrogen operation of the negative ion source. In the hydrogen operation of the surface-produced negative ion source, an ion-ion plasma was

formed in the vicinity of the PG with the same amount of surface-produced negative hydrogen ions and positive ions supplied from the driver region. The amount of negative hydrogen ions was maintained in the enhanced filter condition, owing to the surface production by energetic hydrogen neutrals. The positive ion influx was reduced by the enhanced filter, however the electrons are not increased if there are enough negative ions. The mutual neutralization reaction between negative and positive ions should be decreased in the enhanced filter condition, that is the cause of increase in hydrogen negative ion current. In the deuterium discharge, the negative ion density at the center of the ion source was almost the same as that in the hydrogen discharge, although the deuterium positive ion density was observed to increase by a factor of 1.8 for hydrogen positive ions [25]. Therefore, ion-ion plasma was not formed in the deuterium discharge, and charge neutrality in the vicinity of the PG was maintained by increasing electrons from the driver region. When the positive ion influx is suppressed by enhancing the external magnetic filter, the amount of electrons can be decreased to maintain charge neutrality. For this reason, the enhanced external magnetic filter, using the outer iron yoke is effective in reducing the electron current in the deuterium operation. Similar suppression of the I_e has been observed in the enhanced PG filter in the RF negative ion source for ITER [26]. Therefore, suppression of the I_e in isotope negative ion beams can be efficiently produced by designing the ion source according to the conditions of isotopes with large mass numbers.

Acknowledgments
The authors would like to thank Dr. Fujiwara (NTT) and the technical staff of NBI in NIFS for their maintenance work and operational support. We also thank Dr. Kisaki (QST) for the significant contributions on the accelerator design which he has made it in the past at NIFS. This research is supported by the budget for the NIFS No. ULRR702.

References

[1] Iiyoshi A *et al* 1999 *Nucl. Fusion* **39** 1245
[2] Takeiri Y *et al* 2000 *Rev. Sci. Instrum.* **71** 1225
[3] Tsumori Y *et al* 2004 *Rev. Sci. Instrum.* **75** 1847
[4] Ikeda K *et al* 2019 *Nucl. Fusion* **59** 076009
[5] Ikeda K *et al* 2019 *Rev. Sci. Instrum.* **90** 113322
[6] Kuriyama M *et al* 1998 *J. of Nucl. Sci. and Technology* **35** 739 - 749
[7] Kojima A *et al* 2011 *Nucl. Fusion* **51** 083049
[8] Hiratsuka J *et al* 2020 *Review of Scientific Instruments* **91** 023506
[9] ITER project (*https://www.iter.org*)
[10] Hemsworth R *et al* 1996 *Rev. Sci. Instrum.* **67** 1120
[11] Hemsworth R *et al* 2008 *Rev. Sci. Instrum.* **79** 02C109
[12] Singh M J *et al* 2017 *New J. Phys.* **19** 055004
[13] Kovari M *et al* 2018 *Nucl. Fusion* **58** 026010
[14] Kojima A *et al* 2017 *Fusion Engineering and Design* **121** 145 - 151
[15] Osakabe M *et al* 2018 *IEEE Transactions on Plasma Science* **46** 2324 - 2331
[16] Ikeda K *et al* 2018 *AIP Conference Proceedings* **2011** 060002
[17] Tsumori K *et al* 2010 *Fusion Science and Technology* **58** 489 - 496
[18] Takeiri Y *et al* 2010 *Rev. Sci. Instrum.* **81** 02B114
[19] Ikeda K *et al* 2021 *AIP Conference Proceedings* **2373** 060001
[20] Tsumori K *et al* 1995 *Fusion Engineering and Design* **26** 473 -483
[21] Tsumori K *et al* 2021 *Proc. 28th IAEA Fusion Energy conference (virtual event)* TECH/3-4Rb, to be published Nucl. Fusion in press https://doi.org/10.1088/1741-4326/ac2d59
[22] Inoue T *et al* 1989 *Nuclear Instruments and Methods in Physics Research B* **37/38** 111 - 115
[23] Kuroda K *et al* 1996 *Review of Scientific Instruments* **67** 1114 - 1119
[24] Opera Simulation Software (*https://www.3ds.com/products-services/simulia/products/opera/*)
[25] Masaki S *et al* 2020 *Review of Scientific Instruments* **91** 013512
[26] Speth E *et al* 2006 *Nucl. Fusion* **46** S220 - S238